Performance of Steel Frames with New Lightweight Composite Infill Walls under Curvature Ground Deformation

Wei Xie[1, 2, 3], Junwu Xia[1, 3], Yuying Zheng[2], Qiufen Wang[2], Hongfei Chang[1] and Shangtong Yang[4]

[1] *School of Mechanics and Civil Engineering, China University of Mining and Technology, Xuzhou, China*
[2] *Xuhai College, China University of Mining and Technology, Xuzhou, China*
[3] *Jiangsu Collaborative Innovation Center for Building Energy Saving and Construction Technology, Jiangsu Vocational Institute of Architectural Technology, Xuzhou, China*
[4] *Department of Civil and Environmental Engineering, University of Strathclyde, Glasgow, G1 1XJ, United Kingdom*

ABSTRACT:

In this paper, the structural performance of steel frames with novel lightweight composite infill walls is experimentally and numerically investigated under curvature ground deformation, which is a common consequence of ground mining activities that can cause significant effects on structures and buildings in these areas. A new structural form that combines steel frames and lightweight composite infill walls has recently been used; its performance under curvature ground deformation is of great interest but still not entirely clear. This study compares the mechanical behavior of the open-frame, the closed-frame with mudsill, and the closed-frame with infill walls, through experimental testing under positive and negative curvature ground deformations. Structural responses such as basement counterforce, additional strains at different key locations, and effects of mudsill and infill walls are evaluated. In addition, 3D finite element models are established to simulate the performance of the tested samples and are validated by comparing the results against those from experiments. After validation, the numerical model is applied to a few complex structures incorporating the composite infill walls to investigate their structural performance under both positive and negative curvature ground deformation. It has been found that steel frames with the new composite infill walls can considerably increase the stiffness of structures in resisting ground deformation and re-distribute the loads amongst the beam and column members in the frame. Failure modes for the structures can also be changed by shifting the most dangerous ones from the upper part of the frame to the lower part. Moreover, it has been found that the vertical force of the infill walls is more sensitive to curvature ground deformation than the horizontal force. Further, the influence of the infill wall on the column is more significant, in comparison to that on the beam of the frame.

Keywords: Curvature Ground Deformation; Steel Frame; Infilled Wallboard; Mudsill, Experimental Testing; Finite Element Analysis; Structural Response.

1. INTRODUCTION

Steel frame structures with infill walls have been widely used in civil engineering construction as an important structural type. The infill wall work together with steel frame to provide an efficient structural resistance to applied loads. Recently, in light of sustainable development in construction materials and structures, lightweight, green and functional walls are used as infill walls of steel frame to replace the traditional brick/masonry/concrete walls. Autoclaved lightweight concrete (ALC) is a porous concrete made of calcareous material (cement, lime), silica material (fly ash, sand, etc.) and aluminum powder or paste as gas-producing material, cured at high temperature and pressure and then autoclaved. The ALC has the characteristics of high specific strength (cube compressive strength of about 4 MPa and density of about 500kg/m^3). The panel made of ALC has good performance in fire resistance, sound insulation and heat insulation and thus works as excellent environmental protection wall material with high quality and low price. A new infill wall has been derived which connects two ALC slabs with honeycomb paper boards. This composite wall can massively reduce the selfweight of the wall structure (usually in the range of 72-96%) and the cost, increase the domestic area of the building and have higher heat insulation property. Therefore, to incorporate this new type of infill walls with steel frames can make great impact in the industrial application and produce commercially promising benefits. Meanwhile, ground deformation is a common consequence of underground activities, e.g., mining, water table change, tunneling, crustal movement [1]-[3]. The ground deformation can cause damage to the structures above the ground due to the imbalanced supporting from the foundation. Such a problem is especially significant in the areas that are prone to ground deformation, e.g., mining district (ground deformation caused by mining activities and the diagram of building under curvature ground deformation are shown in Figure 1). However, it is still not entirely clear much clear with regard to the understanding of the structural performance of the steel frame buildings with infill walls which are subjected to ground deformation. This results in major challenge in the design and safety assessment of these structures.

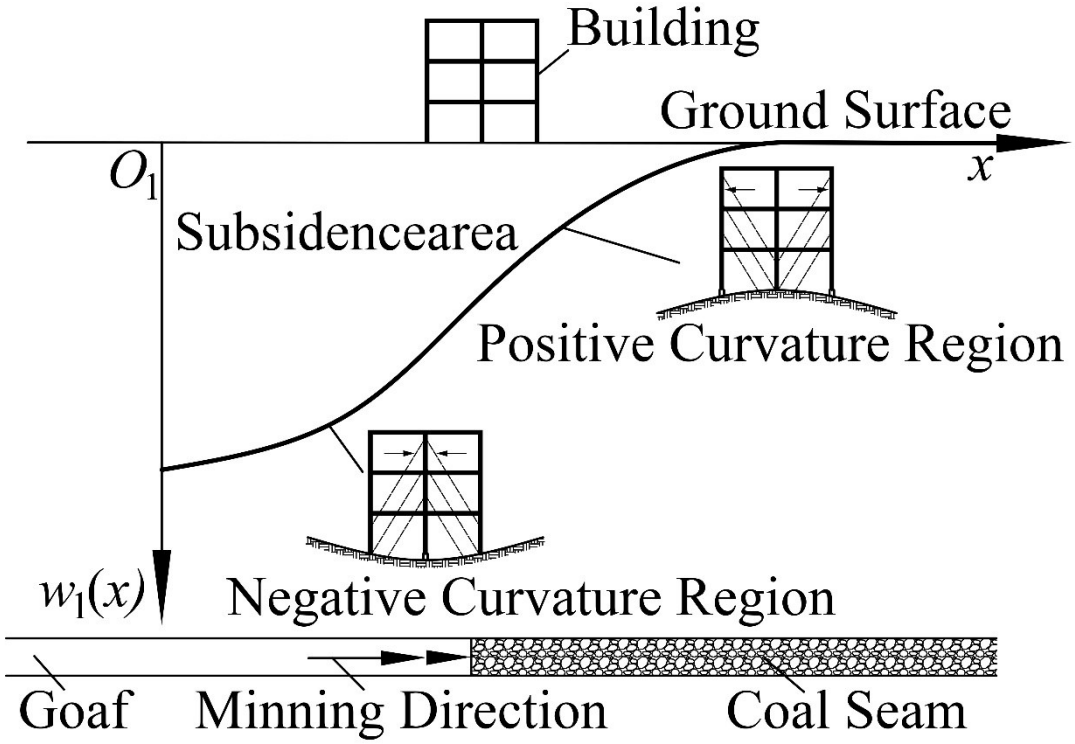

Figure 1. Ground deformation caused by mining and the diagram of building under curvature ground deformation

In the context of increasing industrial applications of steel frame buildings in ground deformation regions, a number of studies on the ground deformation resistance of steel frames have been reported (e.g., [4]-[7]). Meanwhile, the wall component plays an import role in the structural frame performance and thus has attracted considerable research interest. The steel frame infilled with masonry walls were investigated, and a number of the influencing factors, such as thickness of the wall, wall material, wall section shape and the connection type of the wall-frame, on the bearing capacity of the steel frame structure were examined [8]. Through a full-scale dynamic testing of six layers of steel frame infilled with Autoclaved Cellular Concrete (ACC) wall, the natural frequency, damping ratio, and modes were measured, and the results indicated that the lateral stiffness of the steel frame was an improved attribute of the ACC wall [9]. De Matteis [10] studied the seismic effects of sandwich panels on seismic energy–dissipation and lateral resistance of steel structures. Aref and Jung [11] researched the seismic behavior of the system composed of steel frames and Polymer Matrix Composite-infill (PMC) wallboards, analyzed its stiffness and energy dissipation capacity and then found out that the energy dissipation capacity of the structural system was an enhanced attribute of the PMC wallboard. According to the experimental research of Carradine et al. [12] on steel frame system infilled composite wallboard, the lateral stiffness of the structural system was influenced by the in-plane stiffness of the composite wallboard; however, the bearing capacity and the shearing stiffness of the structural system were influenced by the node strength. Moreover, Mehrabi et al. [13] pointed out that the lateral load resistance of the frame with infilled wall is larger than the sum of the

lateral load resistance of the infilled wall and the frame structure. The structural performance of the frame with an infilled wall is significantly better than that of the open-web frame. Cavaleri and Papia [14] proposed a dynamic method to evaluate the equivalent supporting effect of infilled wall in the frame structure. The influences of the center hole of the masonry-infilled wall on the strength and rigidity of steel frames were studied through Discrete Element Method (DEM) simulation [15]. In addition, the cracking strength of the steel frame with infilled wall was analyzed through experiments and finite element simulation [16]. Further, the basic principle of the natural vibration period of a definite reinforced concrete frame with infilled wall was studied through the 3D finite element model and modal eigenvalue analysis [17]. The influence law of the flexible-connection infilled honeycomb sandwich wall panel on the seismic behavior of the reinforced concrete frame structure was studied through an experimental testing [18]. It has been found that the masonry-infilled wall can influence the rigidity and the bearing capacity of steel frame structures significantly, according to the monotonic loading test [19].

Literature suggests that most studies have so far been focused on the lateral rigidity and the seismic behavior of the wall infilled frame structures. There are very limited researches in investigating the ground deformation resistance of structures, and perhaps none in incorporating the novel honeycomb ALC composite infilled walls. This paper attempts to carry out both experimental testing and finite element analysis (FEA) for a number of steel frames with/without the infilled walls under positive and negative curvature ground deformations. A lightweight, sustainable and heat insulated composite wall is applied to the steel frame, and the performance under different types of ground deformation is experimentally evaluated and compared with the open frames and the closed frames without infilled walls. In addition, 3D FEA is conducted and validated against the experimental results. The verified numerical model is then employed to analyze a few other complex cases to fully understand the behavior of these new composite structures under the curvature ground deformation. The experimental results and numerical models can help structural designers, civil engineers and asset managers in their decision-making regarding the design and assessment of the performance of the steel frame infill wall composite structures subjected to curvature ground deformation.

2. EXPERIMENTAL DESIGN

2.1 Specimen and Materials

The structure tested was a typical single-layer two-span steel frame. The steel Q235 was used (one type of steel in China with the yielding strength f_y=235Mpa). The beam-column sections adopted the

H-shape. The honeycomb sandwich wallboard had a total thickness of 100mm and combined 2 outer-panels which are made of autoclaved lightweight concrete (ALC). The honeycomb core board was manufactured into the honeycomb-shape by paper material, as shown in Figure 2. The geometric parameters of the specimen are listed in Table 1.

Table 1. Geometric Parameters of Frame Specimens (mm)

Frame Geometric Dimension		Section of Column and Beam				Wallboard Thickness Parameters		
Span	Height	flange width	Web width	flange Thickness	Web Thickness	Total	Outer-Panel	Core Board
2000	1100	100	100	8	6	100	5	90

The infill walls were placed and connected into the steel frame through the clamp-plate and bolt-plate on the beam and column, as shown in Figure 2. From the force transmission perspective, this wall–frame connection mode was the rigid point connection and has better integrity and higher compliance with the frame than other infill walls, such as out-hung walls and masonry walls.

3 types of frames were made in terms of the placement of mudsill and/or infill walls, i.e., open frame (OPfr, no mudsill and no infill wall), closed frame (CLfr, with mudsill but no infill wall) and frame with infill wall (WAfr, with mudsill).

2.2 Experimental Apparatus and Loading

The experimental testing was executed on the ground deformation test bed at the Jiangsu Key Laboratory of Environmental Impact and Structural Safety in Engineering, China. Test loading included the fixed load and the curvature ground deformation. The diagrammatic sketch of experimental apparatus is shown in Figure 2. The fixed load included the beam load and the concentrated load at the column pedestal. The first one is two-concentrated force at the quartile point on the frame beam which simulates loads passed to the beam from the floor, while the latter one is used to eliminate the effects of the weight difference of the 3 types of frames on the test results.

The curvature ground deformation was loaded through the displacement–control method. The base of column B was fixed and the bases of columns A&C were descended (positive curvature ground deformation loading) or ascended (negative curvature ground deformation loading) by jacks.

When the positive curvature ground deformation was loaded, the middle-column B was fixed and the side-columns A&C were lowered. Initially, the settlement difference between the side-column and

the middle-column S=0, and the base counterforce of the side-columns F_{AC0} were at maximum. With the step by step loading of the positive curvature ground deformation, F_{AC0} was decreased gradually. When F_{AC0} = 0, the bottom surface of the side-column foundation were separated completely from the loading plate, while the loading stage was terminated. At this moment, the settlement difference between the side-column and the middle-column S reached the maximum S_{max}. The negative curvature ground deformation loading was the opposite to this process. Again the middle-column B was fixed and the side-columns A&C were elevated. At the start, the base counterforce of the middle-column F_B was at the maximum, which was then decreased gradually with the progressive loading of the negative curvature ground deformation. The experimental apparatus are illustratively shown in Figure 3. Considering the characteristics of curvature ground deformation, the ends of each element member are the main locations affected and thus the most dangerous locations. To clearly show the locations where the following strain analysis is conducted, Figure 4 is presented.

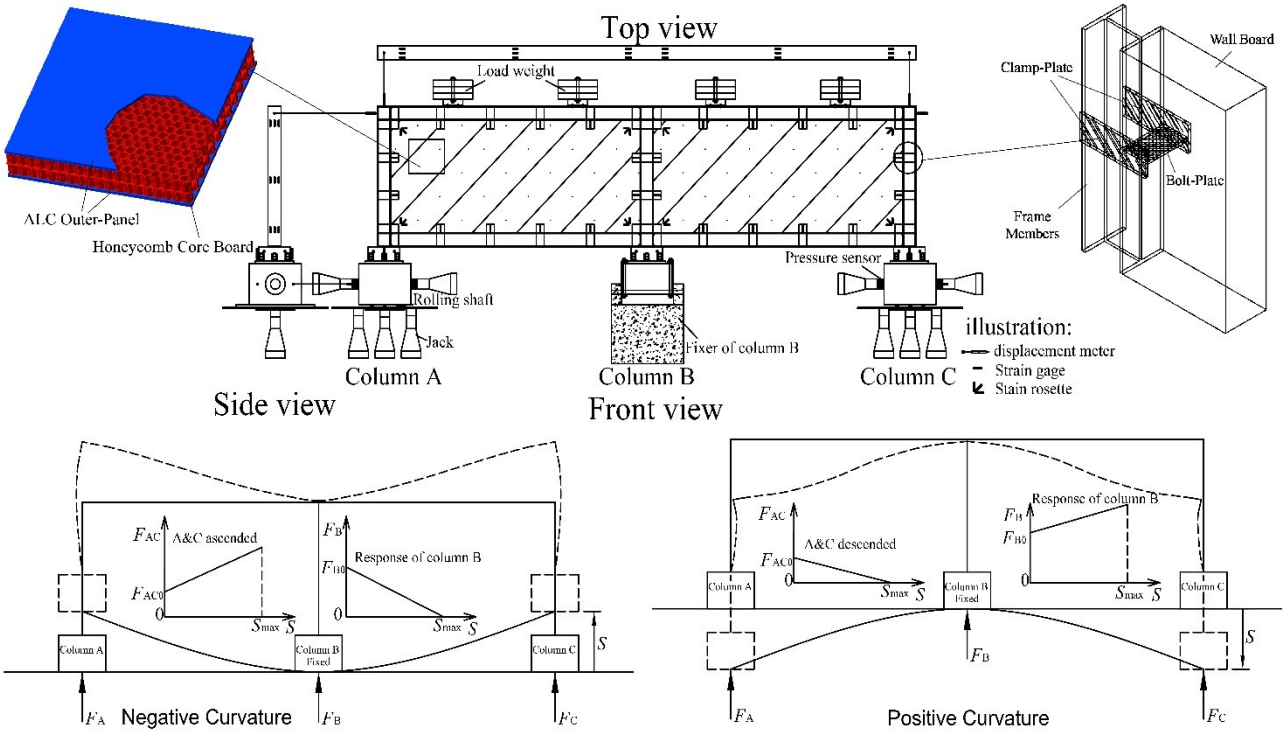

Figure 2. Diagrammatic sketch of experimental apparatus of curvature ground deformation

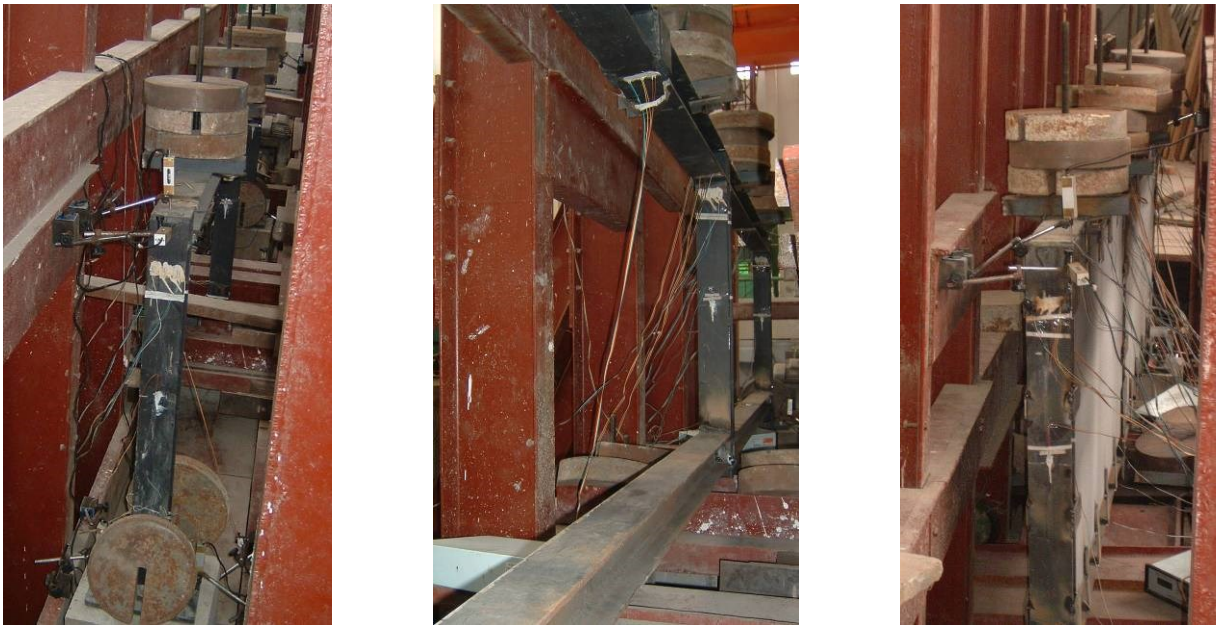

(a) Open Frame (b) Closed Frame (c) Wallboard-Infilled-Frame

Figure 3. Experimental apparatus for ground deformation

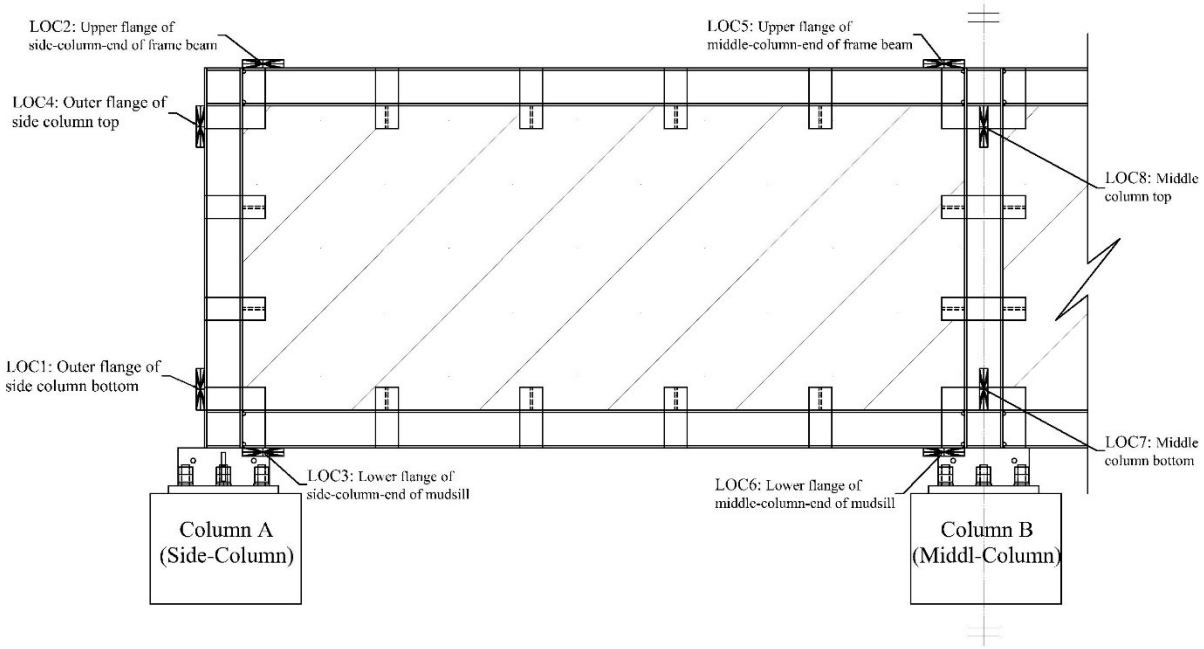

Figure 4. Illustration of some key locations within the frame

3. TEST RESULTS AND ANALYSIS

The counterforces for the side-column under curvature ground deformations for the three structures (i.e., open frame, closed frame and closed frame with infill walls) are compared, and the results are shown in Figure 5. It can be seen that the counterforce of the side columns in the 3 types of frames presents a roughly linear variation with the curvature ground deformation. Meanwhile, under the same displacement loading rate, the WAfr frame shows the maximum variation rate (i.e., the slope)

of the counterforce of the columns, followed by the CLfr and the OPfr respectively. In other words, under the same displacement increment, the variation of basement counterforce is positively correlated with the rigidity of the frame; the WAfr has the largest rigidity compared with the other frames. The comparison of the variation-rates of basement counterforces (i.e., the rigidity) amongst the 3 frames is shown in Figure 6 (PCD means positive curvature ground deformation while NCD means negative curvature ground deformation).

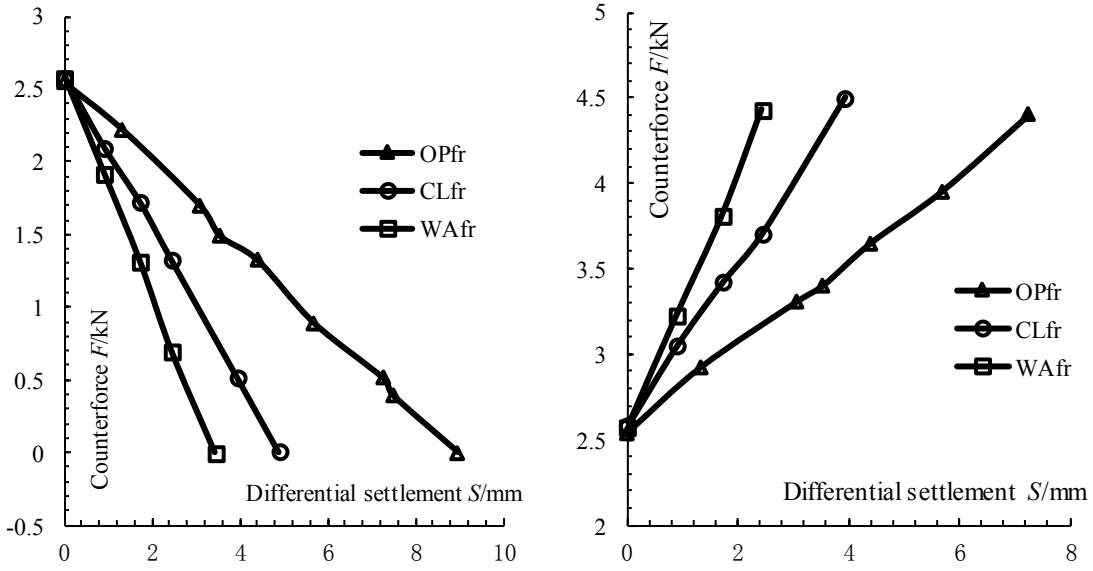

(a) Positive Curvature (b) Negative Curvature

Figure 5. Relation of differential settlement of curvature ground deformation and basement counterforce of side columns

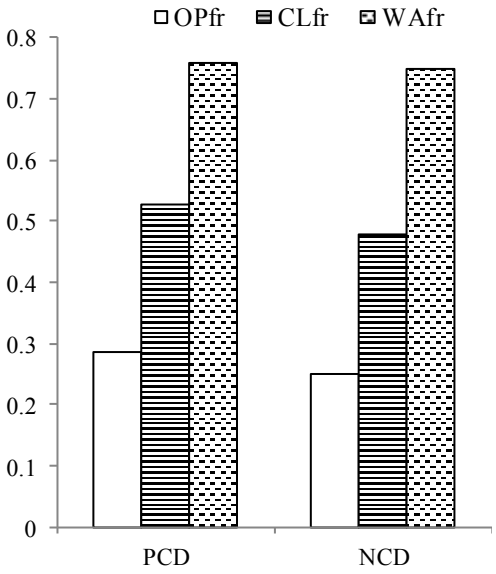

Figure 6. Variation-rates comparison of basement counterforce

It has been seen that the employment of mudsill and infill walls can increase the rigidity of the frame significantly. For the sake of convenience, a relative force parameter D is introduced which represents the difference between the basement counterforce and the initial counterforce ($D = |F - F_0|$). D

presents a proportional relationship with S ($D = kS$, where k is the absolute value of the slope of the F–S linear function). D reflects the curvature ground deformation by the basement counterforce, which can also be called the curvature counterforce.

The additional strain at outer flange of side column bottom (LOC1 shown in Figure 4) in the 3 types of frames under positive and negative curvature counterforce respectively are shown in Figure 7 in terms of the curvature counterforce D. It should be noted that the tensile strain is positive. Figure 7 shows that the strains at the same position of the outer flange of the side column are opposite in sign under the positive and negative curvature counterforces, and they are roughly the same in magnitude. Both strains present a relatively linear growth with the curvature counterforce. It can be seen that the WAfr frame yields the smallest strains for the same counterforce amongst the three frames; however, it is very interesting to see that the closed frame (the one with mudsill) has larger strains than the open frame under the same counterforce. The variation-rate of additional strain at the outer flange of the side columns of the three frame structures are shown in Figure 8. The mudsill increases the strain at the bottom of the side column; however, the infill wall can prevent the increase of the strain development at the same location. The effect of infill wall to the variation-rate of the strain at the bottom of the outer flange of side column is greater than that of the mudsill. This is why the interesting development of strains happens as illustrated in Figure 7, i.e., greater strain for mudsill case but smaller for infill wall case. Furthermore, the influence of mudsill and infill wall on the variation-rate of the strain of side column is slightly bigger under the negative curvature deformation than that under the positive curvature ground deformation.

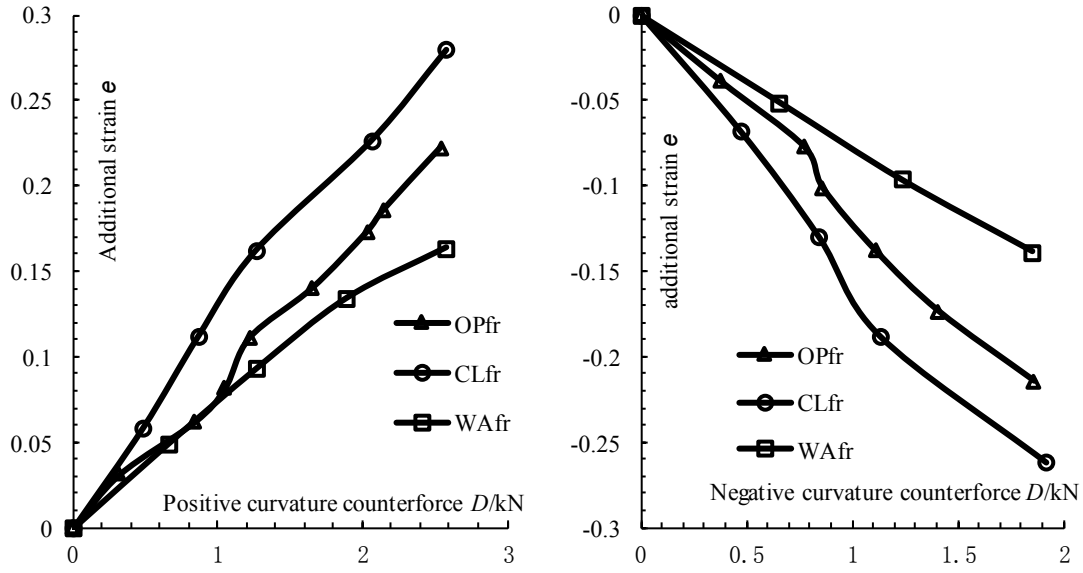

(a) Positive Curvature (b) Negative Curvature

Figure 7. Curvature counterforce-additional strain at outer flange of side column bottom

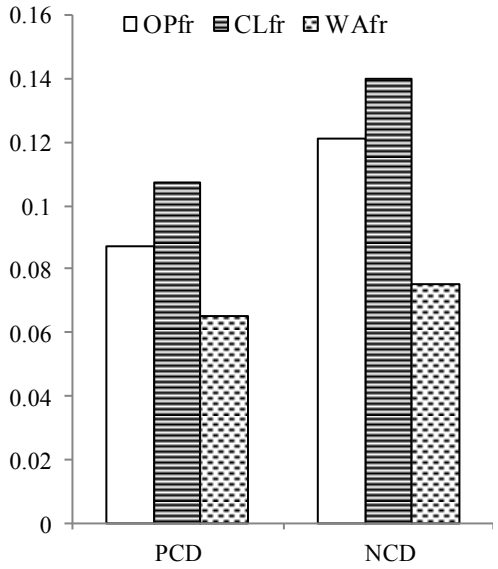

Figure 8. Variation-rates comparison of additional strain at outer flange of side column bottom

The development of strain at the upper flange of side-column-end of frame beam (LOC2 shown in Figure 4) in the 3 types of frames with positive and negative curvature counterforces are shown in Figure 9. The additional strains of the frame beams under positive and negative curvature ground deformations are opposite, and they present a roughly linear growth with the curvature ground deformation. The comparison of the variation rates of the additional strain at the frame beams amongst the 3 types of frames are shown in Figure 10.

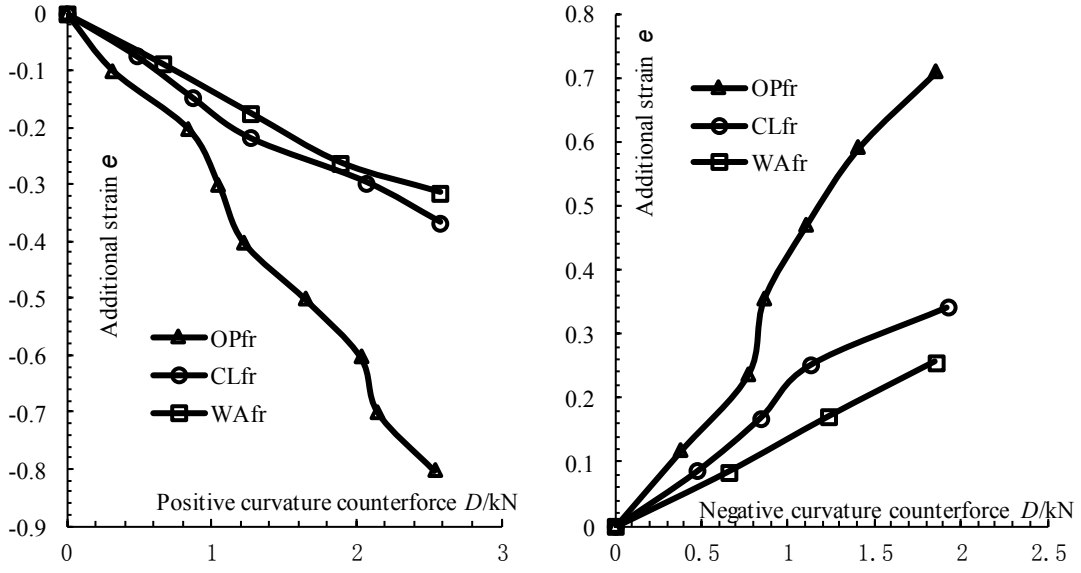

(a) Positive Curvature (b) Negative Curvature

Figure 9. Curvature counterforce-additional strain at upper flange of side-column-end of frame beam

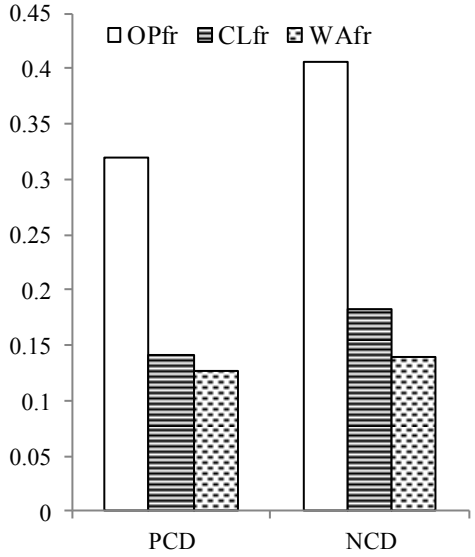

Figure 10. Variation-rates comparison of additional strain at upper flange of side-column-end of frame beam

Obviously, both mudsill and infilled wallboard decelerate the variation of additional strain at the side-column-end of frame beam under positive and negative curvature ground deformations. Mudsill decreases the variation rate of additional strain at the side-column-end of frame beam more significantly than the infilled wallboard. The change of the additional strain at the lower flange of side-column-end of the mudsill (LOC3 shown in Figure 4) of CLfr and WAfr with positive and negative curvature counterforces are shown in Figure 11. A roughly linear growth is obtained under the curvature ground deformation. The comparison of the variation rates of additional strain at the mudsill beam between the 2 types of frames are shown in Figure 12.

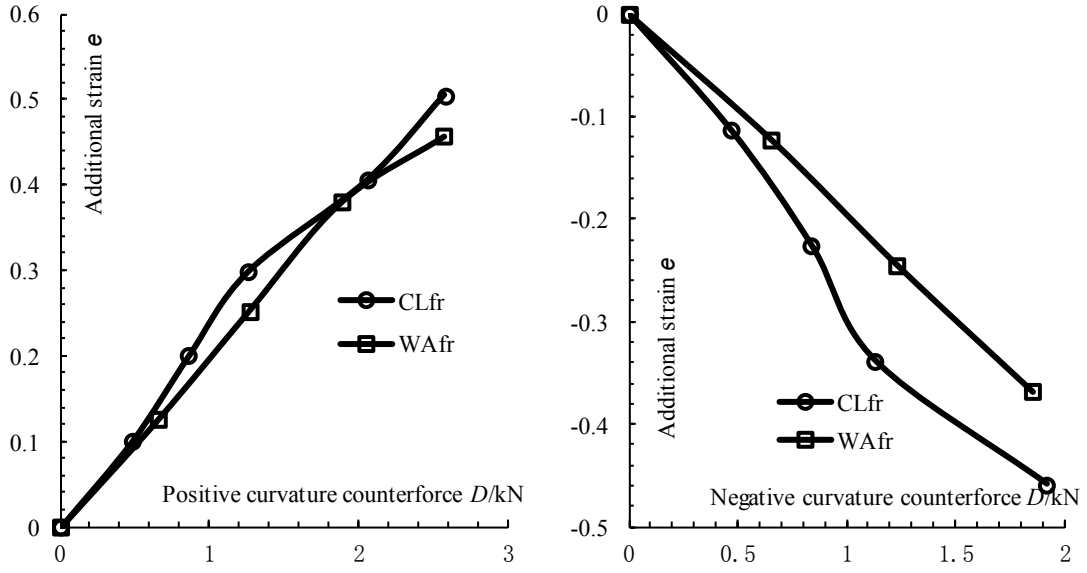

(a) Positive Curvature (b) Negative Curvature

Figure 11. Curvature counterforce-additional strain at lower flange of side-column-end of mudsill

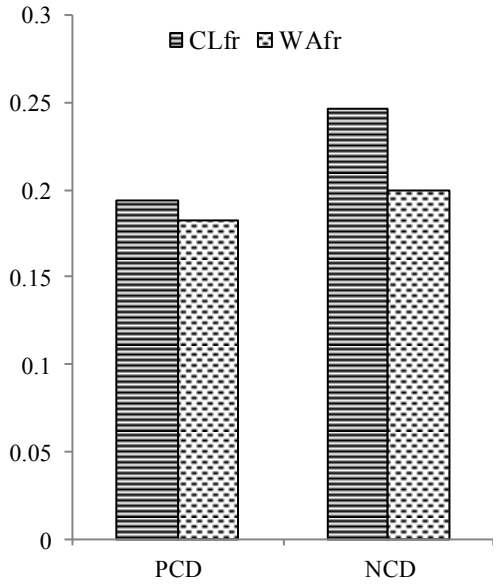

Figure 12. Variation-rates comparison of additional strain at lower flange of mudsill side-column-end

4. FINITE ELEMENT MODEL

According to the experimental testing, there is no obvious plastic stage during the loading process of the ALC outer-panel of the infill wall. It is considered that the infill wall only works in the elastic range and no plasticity and creep of the wall are modeled. In addition, the thickness of the wall panel is relatively small compared with other sizes. As such, a 4-node 6 DOF elastic shell element is used to simulate the ALC outer-panel, and a 2-node 3D spring-damper element is used to simulate the honeycomb core board, as shown in Figure 13.

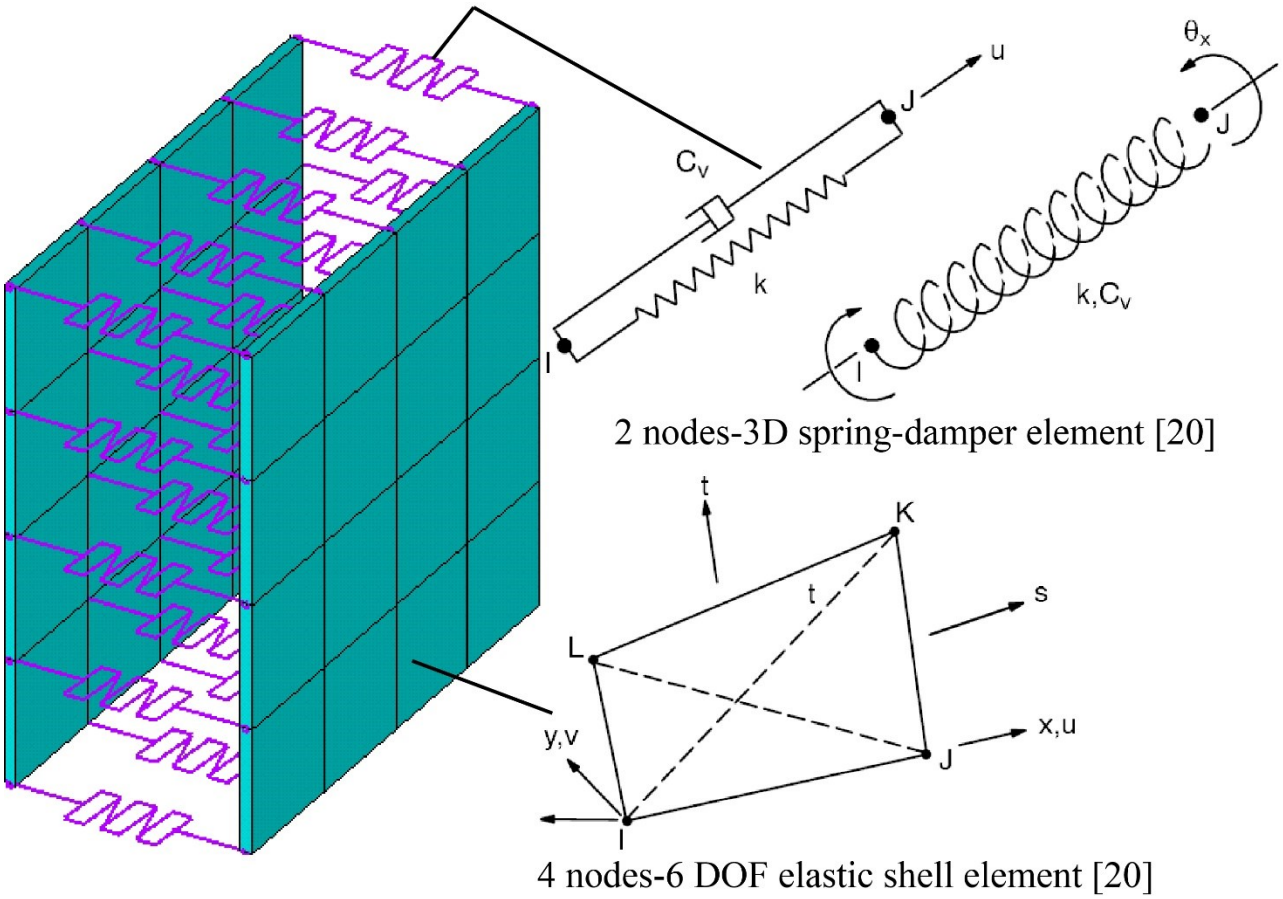

Figure 13. FEA model of honeycomb sandwich wallboard

For the infill walls, the elastic modulus *E* of the ALC panel and the axial spring stiffness *K* of spring-damper element are determined by in-plane and out-plane compression tests of honeycomb sandwich wallboard, respectively. The load-deformation curve and key parameters results of wall boards under in-plane and out-plane compression tests are shown in Figure 14. In this study, the wallboard and frame components are connected through the ALC outer-panel. The honeycomb core panel is subjected to smaller force due to the deformation of the ALC outer-panel, and there is no significant shear effect between the outer-panel and core-panel. This is also proved in experimental observation. Therefore, the interfacial shear behavior of composite wallboard does not have a significant effect on the structural response and is not considered in this study.

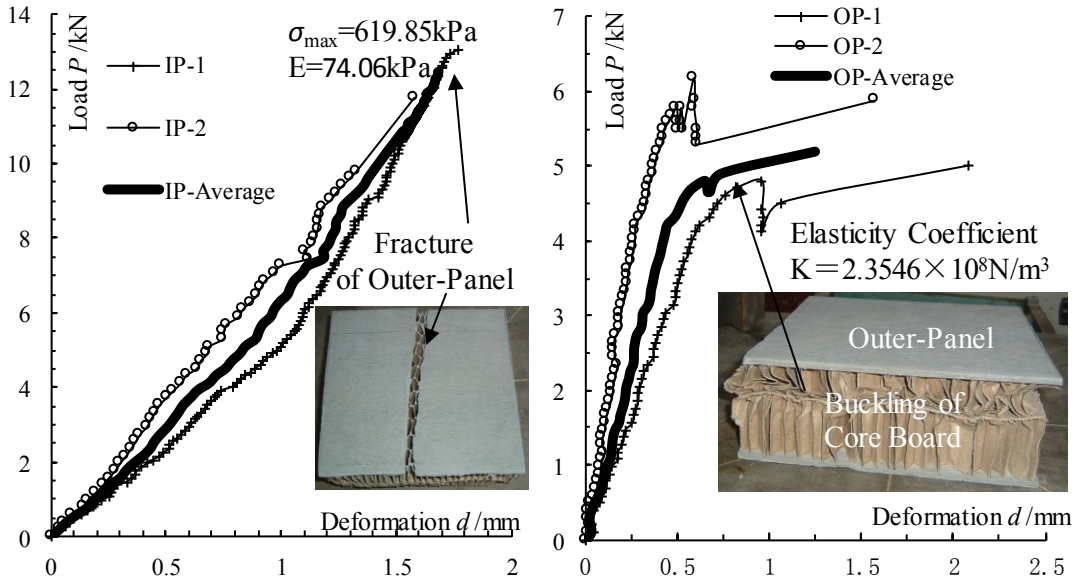

(a) in-plane compression test (b) out-plane compression test

Figure 14. Load-deformation curve of wallboard compression tests

To compare with the experimental testing, three FE models are constructed (namely, FE-OPfr, FE-CLfr and FE-WAfr, respectively). The beam and column adopts 2-node 3D finite strain linear beam element with 6 DOF for each node; and bilinear isotropic hardening model is used for the properties of steel material of the frame. According to the characteristic of wallboard–frame connection mode, the rigid connecting area is small and arranged in a discrete distribution. Therefore, in this paper, the wall–frame connection is achieved or modeled as follows: the edge of wallboard outer-panel element coincides with the inner flange of the beam or column element; 3 translational DOF (U_x、U_y、U_z) of the node of beam or column element and the node of the wallboard outer-panel element are kept in accordance by the way of node coupling in the connection areas. The model can be illustrated in Figure 15 which only shows FE-WAfr as an example.

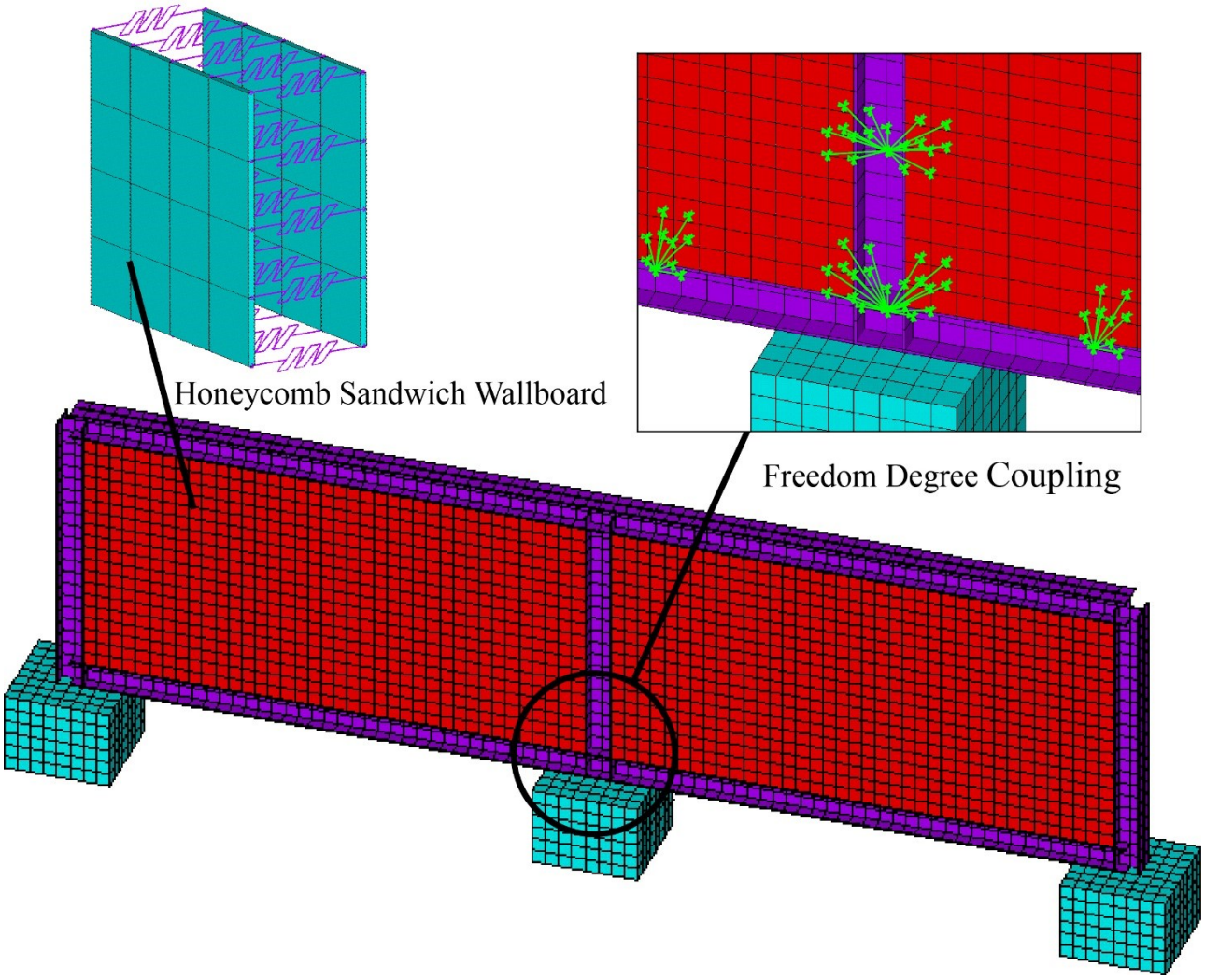

Figure 15. FEA model of physical test frame specimen (fe-wafr: closed frame with infill walls)

Other than the frames established for comparison with the experiments, multi-storey frames are also modeled to investigate the structural performance for more complex and practical structures. As can be seen in Figure 18, three multi-storey frames are built for open frame (FSOP), closed frame with mudsill (FSCL) and closed frame with both mudsill and infill walls (FSWA). Each individual frame spans 6000mm and the height for it is 3300mm.

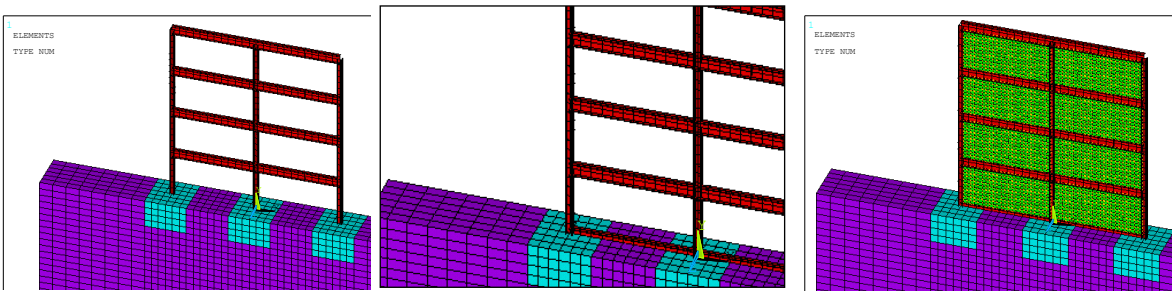

a. FSOP b. FSCL c.FSWA

Figure 16. Finite Element Models for Full-Size Frames

In the full-size frame model, the beam and column are rigidly connected. Also, the column bases are rigid-jointed to the foundation by establishing the constraint equation. The connection between the wallboard and frame members is of discrete-rigid-point-connection by node coupling as that in the test frame model. The ground deformation caused by underground mining activities is a slow process (about 50mm per month). The response of structure under ground deformation in this study is modelled as static process.

5. VALIDATION AND ANALYSIS

5.1 Verification of the Numerical Model

The results obtained from the FEA are verified against those from the experimental testing to validate the numerical model. The in-plane and out-plane compression forces of the wallboard obtained by FEA and experimental testing are compared as shown in Figure 17. It can be seen that the results are in reasonably good agreement. Moreover, the relationship between the counterforce F and the settlement difference S obtained in FEA and experimental testing are compared which are shown in Figure 18. It can be seen they agree well with each other. However, the counterforce obtained in FEA is a little bit larger than that obtained from the test. This is probably because the constraints in the FEA model are theoretically perfect and ideal while the test conditions are not in practice; the different in boundary condition should cause a bit different structural performance. In general, the FEA results are basically consistent with the results of the physical test.

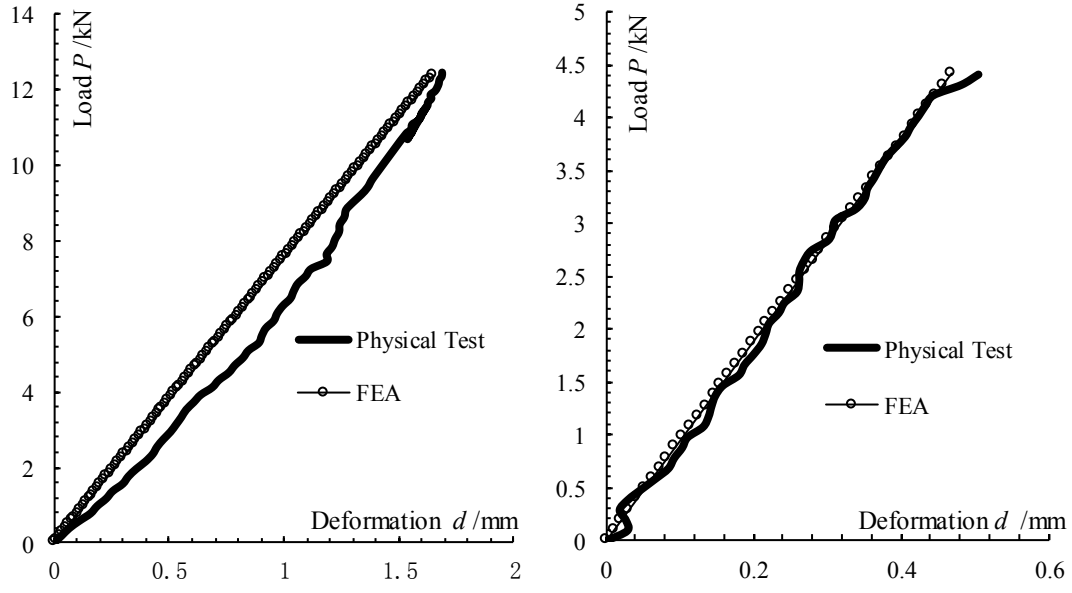

(a) In-Plane Compression (b) Out-Plane Compression

Figure 17. Comparison of wallboard mechanical property between the test and FEA

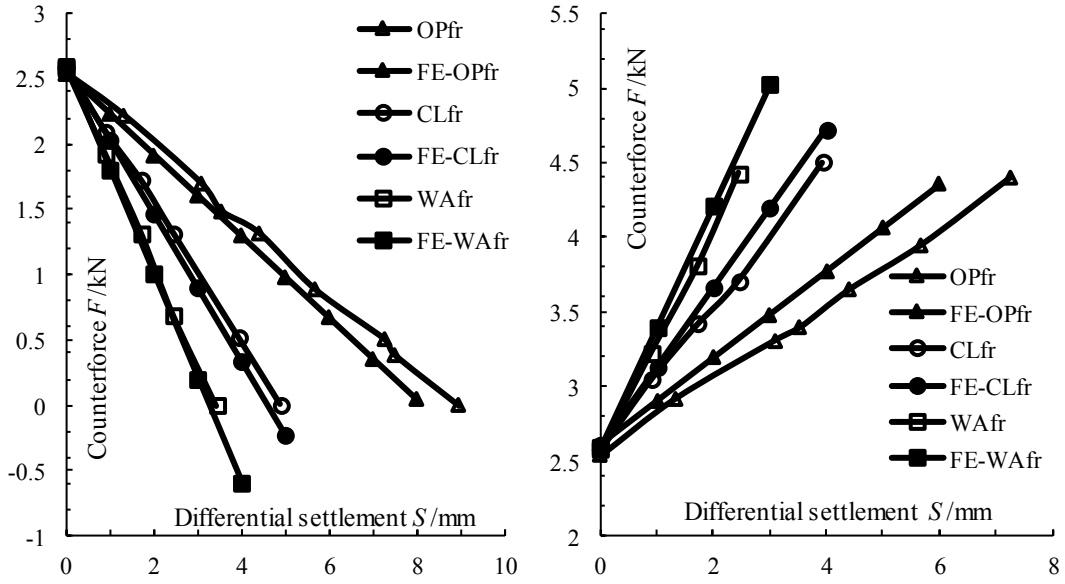

(a) Positive Curvature (b) Negative Curvature

Figure 18. Comparison of counterforce of side columns between the test and FEA

5.2 Failure Analysis

In order to investigate the failure conditions of the 3 types of frames under continuous loading of curvature ground deformation, the displacement loading is applied to the frames in FEA until failure. The dimensionless stress-strength-ratio R is used as the criterion defining the failure of frame members. When R of any member section reaches 1 (marked as R_1), the initial failure of the frame occurs. At the same time, R of the second dangerous section, which is named as R_2, is investigated. The dangerous sections and the corresponding curvature counterforce of the three frames under curvature ground deformation are shown in Table 2.

Table 2. The dangerous sections of frame members under curvature ground deformation

Ground Deformation Type	Failure Information	OPfr	CLfr	WAfr
PCD	R_1	Middle-Column-End of Frame Beam	Middle-Column-End of Mudsill	Middle Column Bottom
	R_2	Side Columns Top	Side-Column-End of Mudsill	Side-Column-End of Mudsill
	Curvature Counterforce D /kN	13.63	27.09	418.54
NCD	R_1	Middle-Column-End of Frame Beam	Side-Column-End of Mudsill	Middle Column Bottom
	R_2	Side Columns Top	Middle-Column-End of Mudsill	Middle-Column-End of Mudsill

	Curvature Counterforce D /kN	14.31	27.10	421.16

The stress-strength-ratio *R* of the 3 types of frames at their own initial failure section varies with the curvature counterforce, as shown in Figure 19.

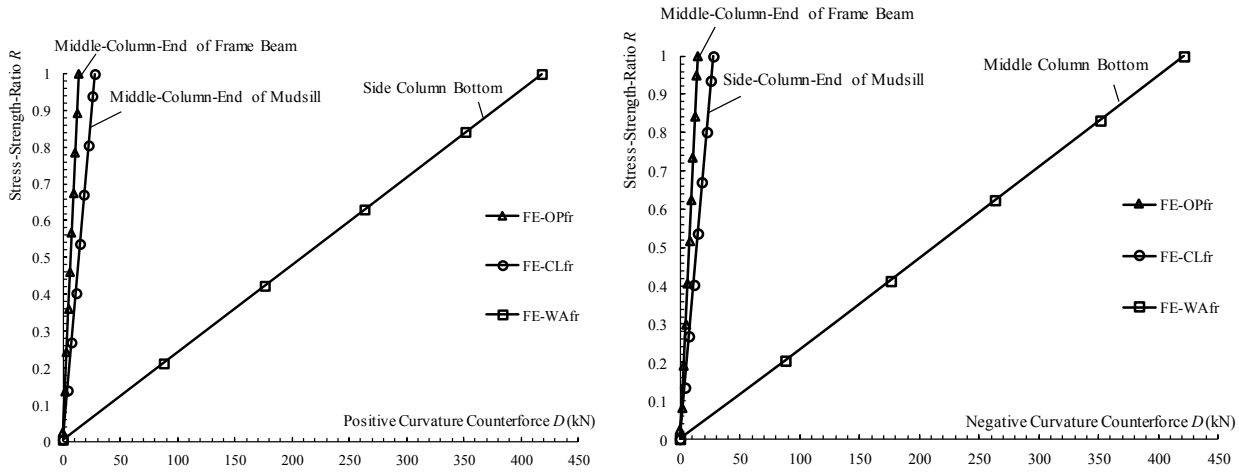

(a) Positive Curvature (b) Negative Curvature

Figure 19. Stress-strength-ratio varies with curvature counterforce of initial failure section of frames

The calculated results show that the stress-strength-ratio *R* of the dangerous sections in Table 2 is linear with the curvature counterforce. The increasing rates of *R* with curvature counterforce of the 5 dangerous sections in 3 types of frames are investigated, as shown in Figure 20.

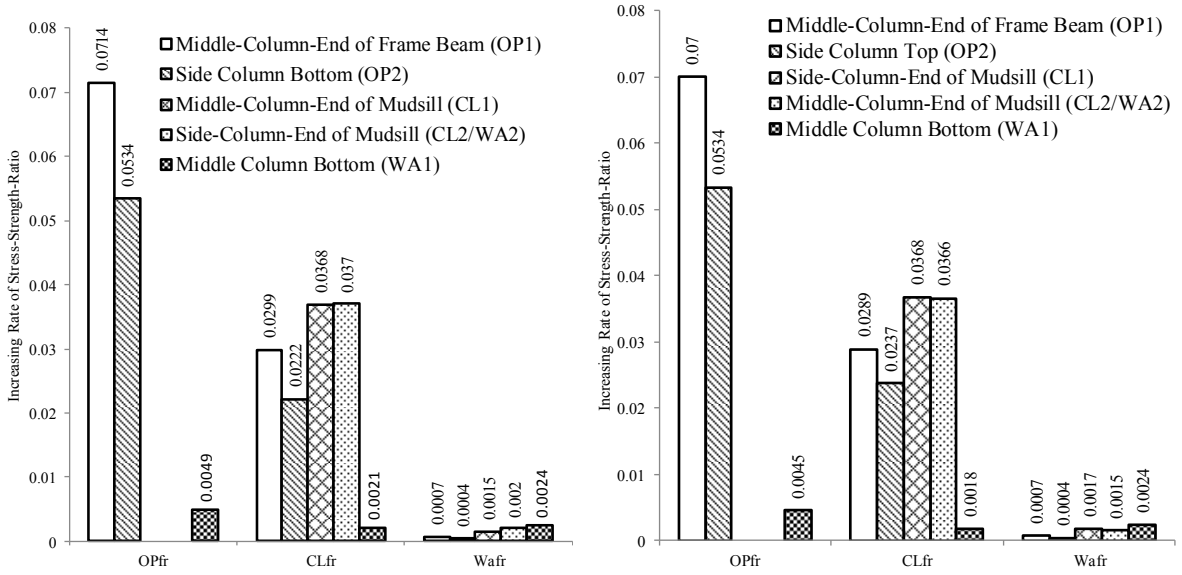

(a) Positive Curvature (b) Negative Curvature

Figure 20. Comparison of increasing rate of stress-strength-ratio with curvature counterforce of dangerous sections

Compared with the positive and negative curvature ground deformation, the mudsill and infilled

wallboard change the initial damage section and the dangerous section of the structure, and the damage and dangerous sections of the CLfr and WAfr are similar. Both the mudsill and wallboard decrease the rate of the stress-strength-ratio *R* increasing with the curvature counterforce. The increase rate of *R* is reduced to some extent by mudsill, which is 46% lower than that of the OPfr, while the rate is decreased significantly by wallboard, which is 97% lower than that of the OPfr. It indicates that the failure rate of the frame under the curvature ground deformation is reduced by mudsill and wallboard, and the effect of wallboard is particularly significant.

When the initial failure of frames occurs, the stress strength ratio of the 5 dangerous sections in Table 2 of the three frames are compared and shown in Figure 21.

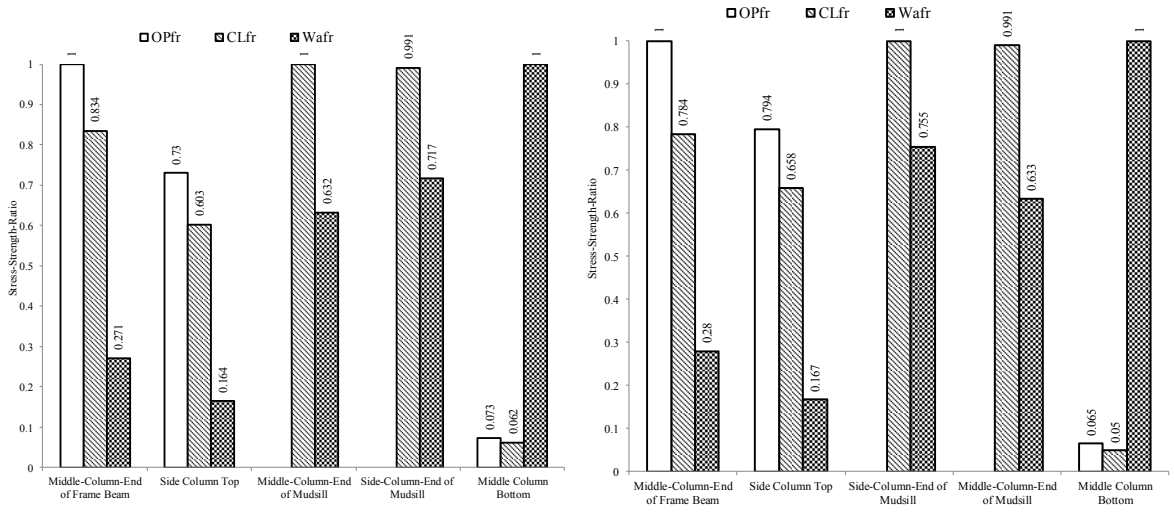

(a) Positive Curvature (b) Negative Curvature

Figure 21. Comparison of stress-strength-ratios of dangerous sections between frames

From Figure 21, under the curvature ground deformation, the middle-column-end of frame beam and side column top (LOC5 and LOC4 shown in Figure 4) is the initial failure section and second dangerous section in OPfr, and the stress-strength-ratios of which sections are both reduced by about 20% and 70% in CLfr and WAfr respectively when the initial failure of them occurs. In other words, the arrangement of the mudsill and wallboard makes the stress-strength-ratio significantly lower. For the middle-column-end and side-column-end of mudsill which is the dangerous sections for CLfr, the stress-strength-ratio *R* for them are reduced by about 36% and 25% respectively, thanks to the infilled wallboard. Because of the existence of the infilled wallbard, the stress-strength-ratio *R* at the middle column bottom is significantly increased. The *R* at the middle column bottom in WAfr is 13.7 times higher than that in Opfr and 16.1 times higher than that in CLfr. The middle column bottom is changed from the relatively safe section in OPfr and CLfr to the initial failure section in WAfr. According to the results of FEA, for the stress composition of the five dangerous sections mentioned above, the stresses of middle-column-end of frame beam, side-column-top, middle-column-end of

mudsill, and ends of mudsill are mainly caused by bending moment, and the stress of middle-column-bottom is caused by axial force.

The stress-strength-ratios corresponding to the above 5 dangerous sections in the same frame are investigated when the initial failure of each of the 3 types of frames occurs. The standard deviation of the stress-strength-ratios are also calculated and shown in Figure 22.

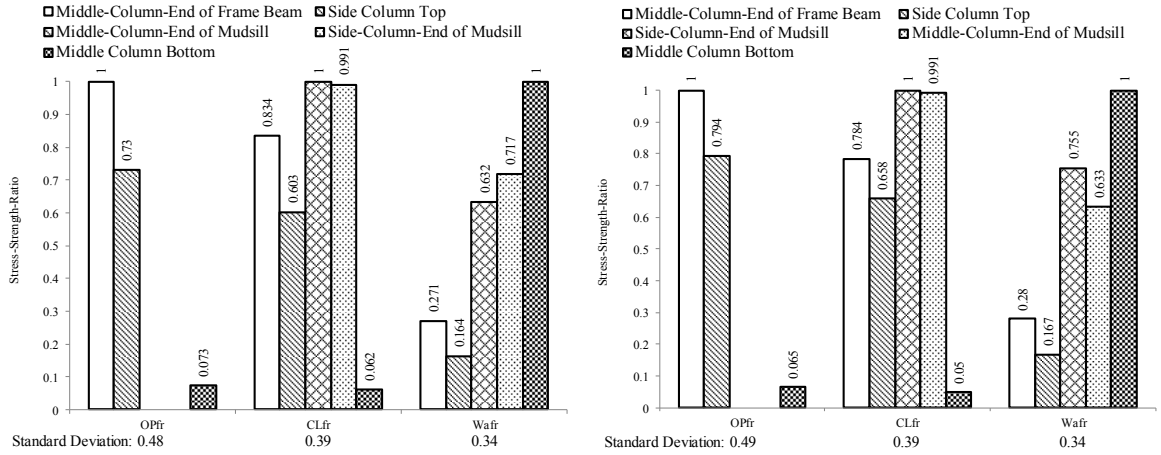

(a) Positive Curvature (b) Negative Curvature

Figure 22. Comparison of stress-strength-ratios between different dangerous sections when initial failure happens

From Figure 22, the presence of mudsill and infilled wallboard shifts the damage and dangerous locations from the upper part of the frame to the lower part. Meanwhile, the standard deviation of the stress-strength-ratio of the above 5 dangerous sections is OPfr > Clfr > WAfr when the initial failure occurs. In other words, the mudsill and infilled wallboard reduce the difference of the stress-strength-ratio distribution so that the distribution of internal force is more balanced. This leads to the most use of the materials.

5.3 Parametric Study and Discussion

A parametric study on the effects of the material choices for the infill walls is carried out in terms of the modulus E of shell element for the concrete board and the elastic coefficient K of the spring-damper element for the honeycomb boards. It has shown that the in-plane stress performance of wallboard is controlled by elastic modulus E, while the elastic coefficient K has little effect on it. By contrast, the out-plane stress performance of wallboard is mainly affected by the elastic coefficient of K. The parameters E and K are relatively independent, which affect the mechanical properties in two directions of the wallboard respectively. Moreover, the in-plane load is mainly resisted by the ALC outer-panel; at the same time, the honeycomb core board provides constraint to the outer-panel.

Figure 23 shows the von Mises stress distribution across the infill walls in the multi-storey steel frame. It can be seen that the maximum stress happens at the central bottom column adjacent to the beams when subjected to positive curvature ground deformation loading. However, when the negative curvature ground deformation loading is applied, the maximum stress is at the locations underneath the first floor beams. Symmetric stress distribution against the middle columns has been observed which makes sense since the load and the structure are both symmetric. In addition, for both loading types, the bottom walls are subjected to greater stresses compared with upper walls. Further, it can be obtained that along the height direction, the variation of stresses under the positive curvature ground deformation loading is larger than that under the negative curvature surface loading.

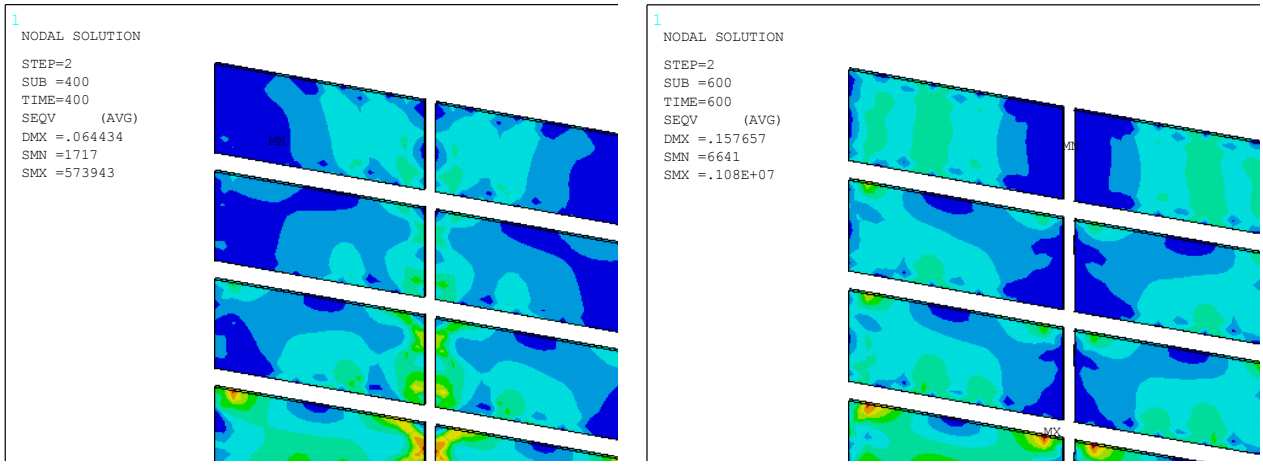

(a) Positive curvature (b) Negative curvature

Figure 23. Von Mises stress distribution in the walls under curvature ground deformation

Figure 24 shows the displacement of the side bottom column, with respect to the middle bottom column, during the change of the curvature surface loading, for the multi-storey frames. Similar to the single storey frames, the closed frames with infill walls are most insensitive to the ground deformation. This means the closed frames with infill walls have the smallest displacement under the same ground curvature loading. It is also interesting to find out that the open frame and the close frame have very close behaviour in both vertical and horizontal directions. It reflects that the mudsill contributes less to the mechanical performance of the multi-storey frames, in comparison to the single storey frames.

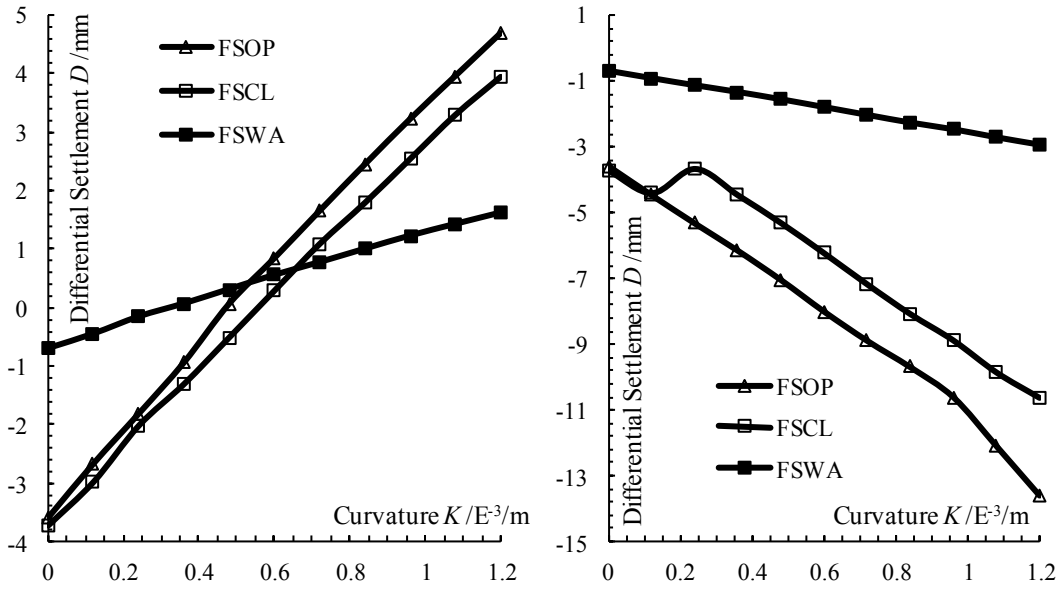

(a) Positive curvature (b) Negative curvature

Figure 24. Side column differential settlement of the multi-storey frames under curvature ground deformation

The moment at the ground floor side column base under curvature ground deformation is shown in Figure 25. The change of the moment for the open frame is massively greater than the closed frame as well as the infilled closed frame. Because of the additional resistance provided from the infill walls, the moment at the corner base can be significantly reduced in comparison with the open frame. The performance under the positive and negative curvature ground deformation are similar, though the directions are opposite. This proves that, by utilising the ALC infill walls, the structural performance of the frames is optimised while the load is more evenly distributed.

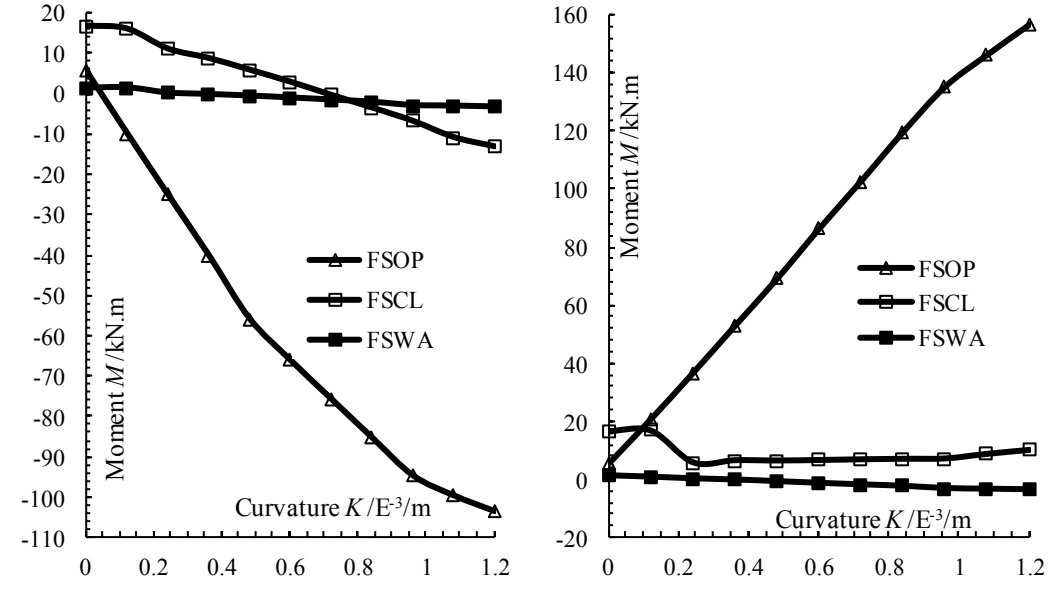

(a) Positive curvature (b) Negative curvature

Figure 25. Moment at the ground floor side column base under curvature ground deformation

The shear force at the ground floor side column base under curvature ground deformation is shown

in Figure 26. Similar to the bending moment, the change rate of the shear force for the open frame is massively greater than the closed frame and the closed frame infilled with ALC walls. At 1.2×10^{-3}/m positive curvature, the shear force at the side column based can reach to 120kN while it is only about 10kN for closed frame and infill wall frame. Under negative (same) curvature, the difference is even higher, i.e., the shear force reaches 225kN for open frame compared to 20kN. The additional resistance to shear mechanism is provided from the infill walls to the frame. The performance under the positive and negative curvature ground deformation are similar and proportionate. These examples demonstrate and justify the significant effect that the ALC infill walls provide to the steel frame in resisting force, moment, stress, displacement, etc., so that more efficient and resilient structures are achieved.

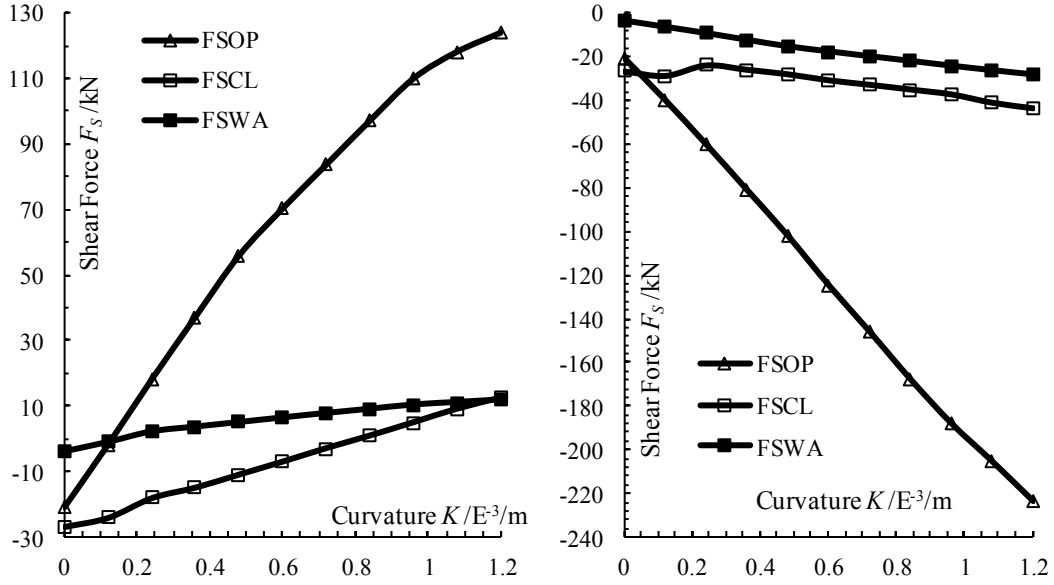

(a) Positive curvature (b) Negative curvature

Figure 26. Shear force at the ground floor side column base under curvature ground deformation

6. CONCLUSIONS

In this paper, the performance of the steel frames incorporated with ALC composite infill walls have been investigated under the curvature ground deformation. Both experimental testing and finite element analysis have been conducted to examine the effects of various parameters on the structural performance. Specifically, the following main conclusions have been obtained:

(1) The settlement and counterforce of the frame are significantly affected by the frame rigidity. The arrangement of mudsill and the ALC composite infill walls can considerably increase the rigidity of the frames and the combination of ALC composite infill walls and the mudsill can provide an optimal enhancement to the rigidity of the frames.

(2) The mudsill and the infill walls can change the location of the initial damage section which move damage and dangerous sections from the upper part of the frame to the lower part; meanwhile, the presence of the infill wallboards significantly increase the stress-strength-ratio at the bottom of the middle column, so that the dangerous parts of the frame moved from the side to the middle. For the design of structures in curvature deformation zone, it is necessary to consider the failure of the key parts and to strengthen the bearing capacity and stability of the members in the middle and bottom regions.

(3) The effect of the mudsill is more significant on the additional strain of the beam of the frame; and the infill wall plays a more considerable role on the additional strain of the column. It is because, under the curvature ground deformation, the columns transmit the basement counterforce to the beam and the beam is the main component that bears the curvature ground deformation. Under the effect of curvature surface deformation, the beams are of great importance and additional care should be taken in the design.

(4) The infill wallboard combines the frame components to work together and forms an integral system which re-organizes the internal stress distribution among beams and columns, thus influencing the additional strain of the frame columns significantly. The vertical force of wallboard is more sensitive to curvature ground deformation than the horizontal force. As such, the vertical resistance of the infilled walls should be strengthened first for buildings in curvature deformation area.

(5) The infill walls reduce the difference of the stress-strength-ratio numerical distribution of each member when the frame is loaded to failure. Therefore, the distribution of internal force is more balanced and the materials are hence fully utilized.

ACKNOWLEDGMENTS

This work was financially supported by the National Science Foundation of China (Grant No. 51274192, 51408596), the Jiangsu Province Science Foundation of China (Grant No. BK20140195), The Natural Science Foundation of the JiangSu Higher Education Institutions of China (Grant No. 16KJB560021), the Qing Lan Project of Jiangsu Colleges and Universities of China, the Open Foundation of Jiangsu Collaborative Innovation Center for Building Energy Saving and Construction Technology Open Foundation of China (Grant No. SJXTQ1617).

REFERENCES

[1] Galloway, D., Jones, D.R., Ingebritsen, S.E.. land subsidence in the United States: U.S. Geological Survey Circular, 1999, 1182.117PP.

[2] Bouwer, H.. Land subsidence and cracking due to groundwater depletion. Ground Water, 1977 15, 358–364.

[3] Annette Klein, Wolfgang Jacoby, Peter Smilde. Mining-induced crustal deformation in northwest Germany: modelling the rheological structure of the lithosphere [J]. Earth and Planetary Science Letters, 1997, 147: 107-123.

[4] Xie Wei, Xia Junwu Zheng Yuying. Experimental study on cooperation of infilled wallboard steel frame under differential settling [J]. Journal of Sichuan University (Engineering Science Edition), 2015, 47(2): 57-63.

[5] Xie Wei, Xia Junwu. Experimental study on co-operation of infilled wallboard-steel frame under ground deformation [J]. Journal of Huazhong University of Science and Technology (Urban Science Edition), 2008, 25(3): 169-171.

[6] Xia Junwu, Yuan Yingshu, Dong Zhengzhu. Mechanics model of ground, independent footing and framework [J]. Journal of China University of Mining and Technology, 2007, 36(1): 33-37.

[7] Xu Xingxing. Study on the internal force calculation methods of semi-rigid steel frames under vertical loads and ground deformation interaction in mining subsidence area [D]. Xu Zhou, China: China University of Mining and Technology, 2015

[8] Karaduman. A., Polat, Z., Kaltakci, M.y.. Statical analysis of infilled frame[J]. Studies, Repairs, and Maintenance of Historical Buildings, 2001, 7: 425-433.

[9] M. Memari, A. A. Aghakouehak, M. Ghafory A Shtiany, M.Tiv. Full-scale dynamic testing of a steel frame building during construction[J]. Engineering Structures, 1999, 21: 1115-1127.

[10] De Matteis, G. Diaphragm action of sandwich panels in pin-joint steel structures: a seismic study [J]. Journal of Earthquake Engineering, 2000, 4(3): 251-275.

[11] Aref AJ, Jung W.Y. Energy-dissipating polymer matrix composite-infill wall system for seismic retrofitting [J]. Journal of Structural Engineering ASCE, 2003, 129(4): 440-448.

[12] Carradine D. M. Woeste F. E. Dolan, J. D. Loferski, J. R. Utilizing Diaphragm action forwind load design of timber frame and structural insulated panel buildings[J]. Forest Products Journal, 2004, 54(5): 73-80.

[13] Mehrabi,A.B., Shing,P.b, .Schuller. Performance of masonry infilled RC frames under in-plane lateral loads[J]. Journal of Structural Engineers, 2002, 122(3): 228-237.

[14] L. Cavaleri, M. Papia. A new dynamic identification technique: application to the evaluation of the equivalent strut for infilled frames[J]. Engineering Structures. 2003, 25: 889-901.

[15] Mohebkhah A., Tasnimi A. A., Moghaddam H.A. Nonlinear analysis of masonry-infilled steel frames using discrete element method[J]. Journal of Constructional Steel Research, 2008, 64(12):1463-1472.

[16] H. A. Moghadam, M. Gh. Mohammadi, M. Ghaemian. Experimental and analytical investigation into crak strength determination of infilled steel frames[J]. Journal of Constructional Steel Research, 2006, 62: 1341-1352.

[17] Khan Mahmud Amanat, Ekramul Hoque. A rationale for determining the natural period of RC building frames having infill [J]. Engineering Structures. 2006, 28: 495-502.

[18] Xia Junwu, Xie Wei, Luo Zexin. Experimental study on frame seismic performance impacted by infilled wallboard [J]. Journal of Huazhong University of Science and Technology (Natural Science Edition), 2012, 40(5): 89-92.

[19] Liu Yushu, Li Guoqiang. Experimental and theoretical research on lateral load resistance of steel frames with infilled walls[J]. Journal of Building Structures, 2005, 26(3): 78-84.

[20] Yang Hong, Chen Jing-ke, Chen Yin-song. Effects of infill walls on nonlinear seismic response characteristics of spatial frames [J]. Journal of Sichuan University (Engineering Science Edition), 2012, 44(5): 38~46.

[21] Li Jianhui, Xue Yantao, Wang Cuikun, et al. Research and development in seismic performance of infilled walls for frame structures [J]. Building Structure, 2011, 41(S1): 12-17.

[22] ANSYS, Inc. Theory Manual. SAS IP, Inc.